Supplementary Information

Stirring-Directed Pathway Selection between 1D Nanofibers and Multilayer Sheet-like Assemblies in Supramolecular Polymerization

Mengmeng Zheng [a] and Chun Liu [a]*

Contents

1. Materials and methods

General. All chemicals and solvents were purchased from commercial suppliers and used without further purification. ^{1}H and ^{13}C NMR spectra were recorded on a 400 MHz Varian DLG400 or a 600 MHz Bruker AVANCE III 600 spectrometer. MALDI-TOF mass spectra were obtained using a Bruker Daltonics Autoflex II LRF/Ultraflex Extreme. UV–vis absorption spectra were recorded on an Agilent Cary 100 spectrophotometer equipped with magnetic stirring and temperature control. Atomic force microscopy (AFM) images were acquired using a Bruker NanoWizard 4 XP. FTIR spectra were measured on a Thermo Fisher 6700 spectrometer. Ultrasonication was performed with a Hielscher UP50H (50 kHz, 50 W). Small- and wide-angle X-ray scattering (SAXS/WAXS) measurements were performed using a Xeuss 3.0.

Synthetic Details and Characterization

Compound **1** was prepared according to reported procedures.[1,2]

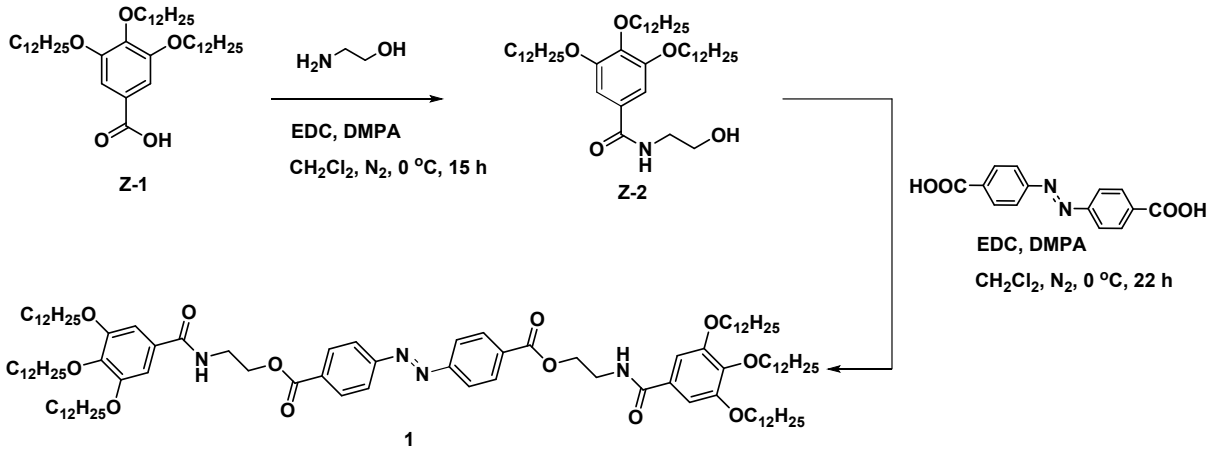

Scheme S1. Synthesis routes of **1**.

Z-2. In a 25 mL round-bottom flask, **Z-1** (340 mg, 0.50 mmol, 1.0 eq), EDC·HCl (115 mg, 0.60 mmol, 1.2 eq), and DMAP (73 mg, 0.60 mmol, 1.2 eq) were added sequentially and purged with nitrogen (3 cycles). Deoxygenated CH_2Cl_2 (10 mL) was added, and the mixture was stirred at room temperature for 45 min before tert-butyl (2-hydroxyethyl)carbamate (42 µL, 0.60 mmol, 1.2 eq) was added. After stirring for 15 h, the mixture was washed with 1 M HCl and brine, then dried over Na_2SO_4. The organic phase was concentrated, and the crude was purified by column chromatography (petroleum ether/ethyl acetate, v/v = 5:3) to give **Z-2** as a white powder (348 mg, 85%). ^{1}H NMR (400 MHz, $CDCl_3$) δ 6.90 (s, 2H), 3.99 – 3.87 (m, 6H), 3.76

(s, 2H), 3.54 (s, 2H), 1.73 (d, J = 14.6 Hz, 6H), 1.39 (t, J = 7.8 Hz, 6H), 1.32 – 1.23 (m, 48H), 0.82 (t, J = 6.4 Hz, 9H).

1. In a 25 mL round-bottom flask, **Z-2** (340 mg, 0.50 mmol, 1.0 eq), EDC·HCl (115 mg, 0.60 mmol, 1.2 eq), and DMAP (73 mg, 0.60 mmol, 1.2 eq) were added sequentially and purged with nitrogen (3 cycles). CH_2Cl_2 (10 mL) was added, and the mixture was stirred at room temperature for 45 min before 4,4-azodibenzoic acid (104 mg, 0.60 mmol, 1.2 eq) was added. After stirring for 15 h, the mixture was washed with 1 M HCl and brine, then dried over Na_2SO_4. The organic phase was concentrated, and the crude was purified by column chromatography (CH_2Cl_2/MeOH, v/v = 40/1) to give **1** as a red powder (65 mg, 55%). ^{1}H NMR (400 MHz, $CDCl_3$) δ 8.22 (d, J = 8.2 Hz, 4H), 7.99 (d, J = 8.2 Hz, 4H), 6.97 (s, 4H), 6.53 (s, 2H), 4.61 (t, J = 5.1 Hz, 4H), 4.06 – 3.92 (m, 12H), 3.87 (t, J = 5.1 Hz, 4H), 1.76 (t, J = 28.7, 6.7 Hz, 12H), 1.46 (t, J = 7.2 Hz, 12H), 1.33 – 1.25 (m, 96H), 0.87 (t, J = 6.8, 2.3 Hz, 18H). ^{13}C NMR (126 MHz, $CDCl_3$) δ 167.79, 161.13, 153.08, 151.92, 141.83, 127.04, 123.06, 122.24, 107.20, 72.55, 68.25, 62.69, 39.15, 30.91, 29.32, 28.72, 28.65, 28.55, 28.39, 28.36, 28.31, 21.68, 13.10. MALDI-TOF-MS (m/z): calcd. for $C_{104}H_{172}N_4NaO_{12}$ $[M+Na]^+$, 1692.2864; found, 1692.2892.

2. Experimental procedures

Sample Preparation

Agg1: Obtained by cooling a monomer solution of **1** in MCH (50 μM) from 353 K to 293 K at 1 K/min under quiescent cooling.

Agg2: prepared under the same cooling conditions but with continuous stirring at 800 rpm.

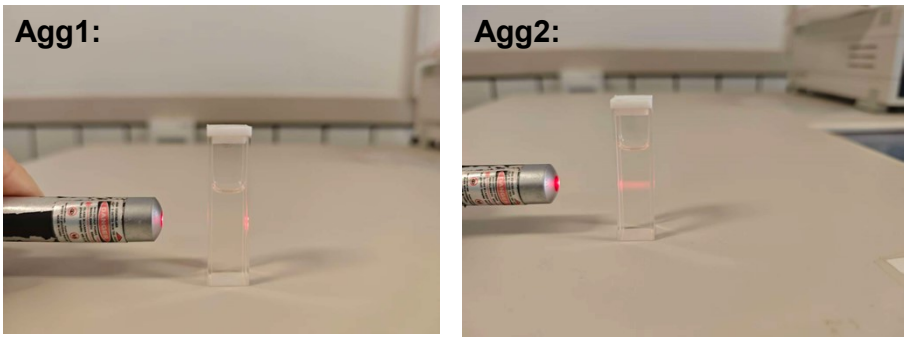

Scheme S2. Photographs of **Agg1** and **Agg2** under laser illumination.

AFM Sample Preparation

A sample of the supramolecular polymer was drop-cast on a silicon wafer, and the solvent was allowed to evaporate under ambient conditions.

Small- and Wide-Angle X-ray scattering (SAXS/WAXS) Measurements

Film preparation: a cast film was prepared by slow evaporation of a concentrated suspension of **Agg1** or **Agg2** (10 mmol/L) in MCH on aluminum foil at room temperature.

SAXS measurements and data processing: SAXS measurements were performed on a Xeuss 3.0 instrument. The scattering from a film prepared under identical conditions was measured and subtracted from the sample signal. The resulting 1D profiles were plotted as $I(q)$versus q. The lamellar repeat distance was calculated as $d = 2\pi/q^*$, where q^* is the position of the lamellar correlation peak.

Thermodynamic Study

The sample of **1** (50 μM in MCH) was prepared in a quartz cuvette and heated to 353 K under magnetic stirring (800 rpm). The absorption spectra were recorded at a cooling rate of 1 K/min and a 30 s delay at each temperature step before measurement.

Denaturation Study

As a representative example, a 1.5 mL suspension of **Agg2** (50 μM, MCH) was prepared in a quartz cuvette. Subsequently, 25 μL aliquots of a solution of **1** (50 μM, $CHCl_3$) were added dropwise to the **Agg2** suspension. After each addition, the mixture was stirred for 30 s (800 rpm) and the UV–vis absorption spectrum was recorded. This procedure was repeated until complete depolymerization to monomers was achieved.

Nucleation–Elongation Model for Cooperative Supramolecular Polymerization

The equilibrium between monomers and thermodynamically favored species can be described as a cooperative process using the Nucleation–Elongation model developed by Eikelder, Markvoort, and Meijer.[3,4] Thermodynamic parameters (ΔH^{o}, ΔS^{o}, $\Delta H_{nucl}{}^{o}$, and T_e) were obtained by non-linear least-squares fitting of temperature-dependent UV–vis melting curves. Thermodynamic parameters were calculated using Eqs. (1)–(4).

Nucleation step : $K_{nucl} = e^{\left(\frac{-((\Delta H^0 - \Delta H_{nucl}^0) - T\Delta S^0)}{RT}\right)}$ (1)

Elongation step: $K_{el} = e^{\left(\frac{-(\Delta H^0 - T\Delta S^0)}{RT}\right)}$ (2)

Cooperativity factor: $\sigma = \frac{K_{nucl}}{K_{el}} = e^{\left(\frac{\Delta H_{nucl}^0}{RT}\right)}$ (3)

Gibbs free energy: $\Delta G^0 = \Delta H^0 - T\Delta S^0$ (4)

Photoisomerization Behavior of Compound 1

The first-order rate constant for the *trans*-to-*cis* isomerization can be calculated from the changes in absorbance of the azobenzene chromophore. Upon irradiation at a wavelength of 365 nm, the azobenzene in compound **1** undergoes *trans*-to-*cis* isomerization. By recording the absorbance change of the *trans* isomer at 328 nm, the first-order rate constant for the *trans*-to-*cis* isomer can be calculated using eq. (5).[5]

$$\ln[(A_\infty - A_t)/(A_\infty - A_0)] = -k_e t \quad (5)$$

where A_∞, A_0 and A_t represent the intensity of the absorption peak at 328 nm at infinite time, time zero and time t, respectively.

Upon irradiation with green light at a wavelength of 530 nm LED, the azobenzene chromophore undergoes isomerization from the *cis*-to-*trans* configuration. The rate constant for this *cis*-to-*trans* isomerization can be calculated by recording the change in absorbance of the *trans* isomer at 328 nm. The first-order rate constant for the isomerization from *cis*-to-*trans* can be determined using the following eq. (6).[6]

$$\ln[(A_\infty - A_t)/(A_\infty - A_0)] = -k_H t \quad (6)$$

Here A_∞, A_0 and A_t represent the intensity of the absorption peak at 328 nm at infinite time, time zero and time t, respectively.

Upon UV irradiation at 365 nm, the absorption spectra became invariant, however, the characteristic *trans*-azobenzene band at 328 nm did not vanish completely. The *trans*-azobenzene fraction was quantified from the absorbance change at 328 nm using eq. (7). [6]

$$trans\% = A_\infty/A_0 \times 100\% \quad (7)$$

where A_∞ and A_0 represent the absorbance at 328 nm at infinite time and at time zero, respectively.

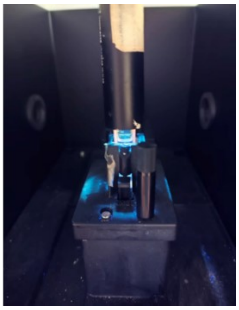

Scheme S3. The instrumental setup for *trans*-to-*cis* photoisomerization under 365 nm irradiation.

3. Supplementary Figures

$CHCl_3$ serves as a good solvent in which compound **1** exists predominantly as monomers. The UV–vis absorption spectrum of **1** in $CHCl_3$ (c = 50 μM) at 298 K exhibited intense, well-defined bands between 250–375 nm, with a maximum at 328 nm. Comparable spectral features were observed in MCH at 353 K, confirming that **1** also remains monomeric under these conditions. Despite its limited solubility in MCH, this solvent could be suitable for the aggregation studies.

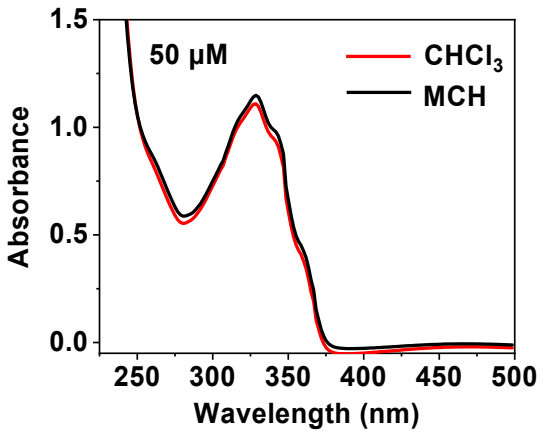

Figure S1. UV–vis absorption spectra of **1** in $CHCl_3$ at 298 K and in MCH at 353 K.

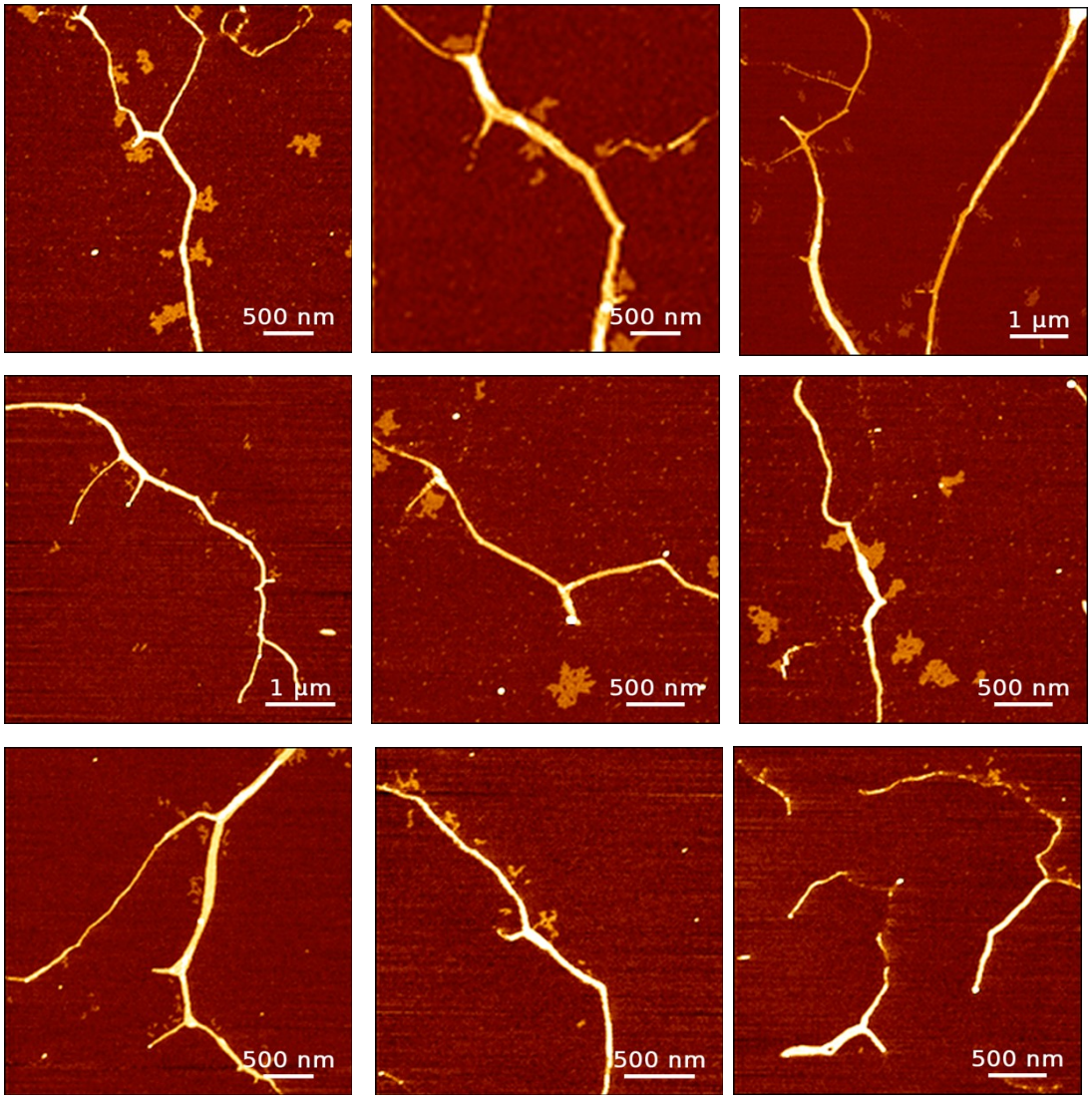

Figure S2. AFM images of **Agg1** in MCH (c = 50 µM) drop-cast on a silicon wafer.

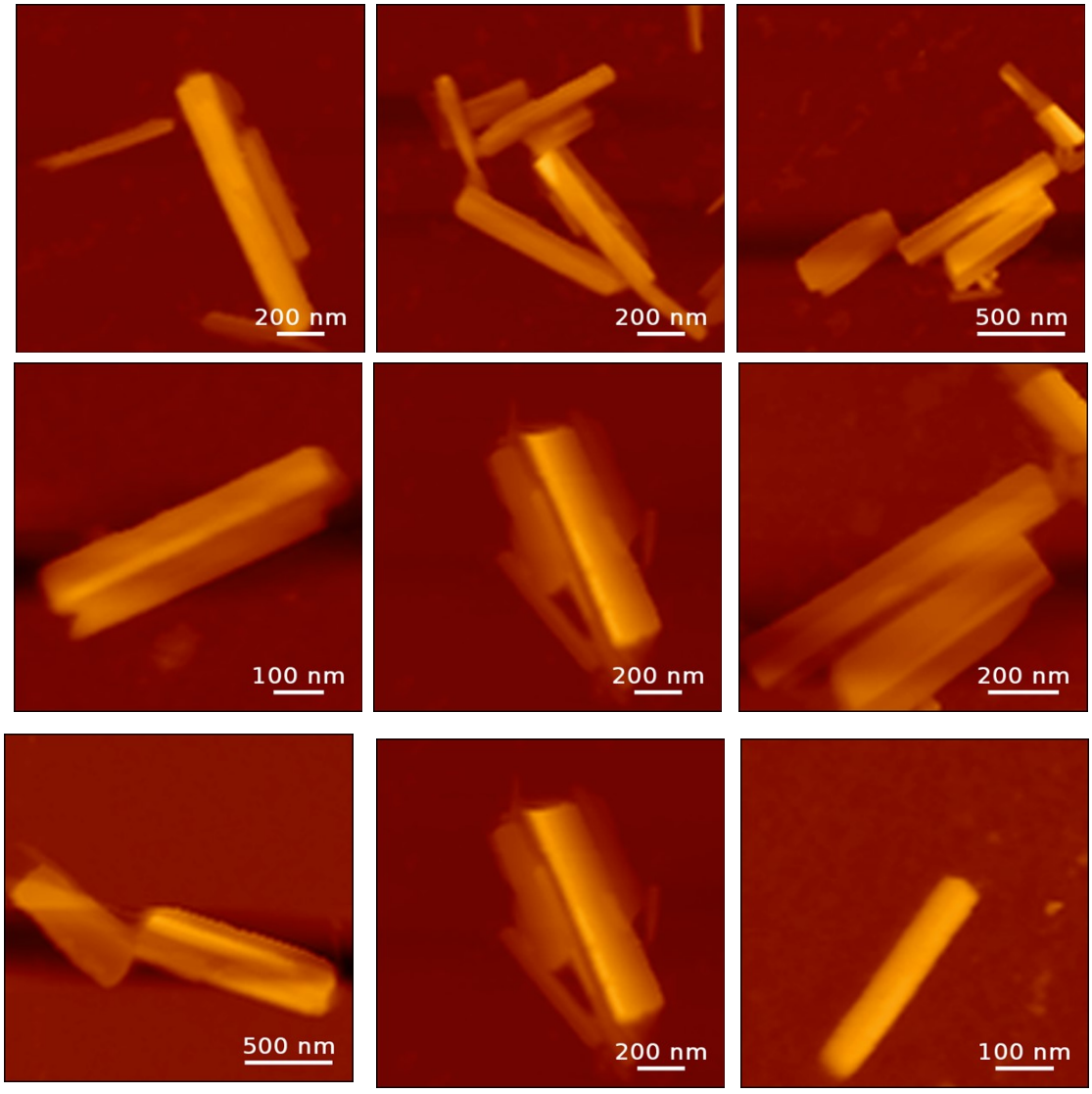

Figure S3. AFM images of **Agg2** in MCH (c = 50 μM) drop-cast on a silicon wafer.

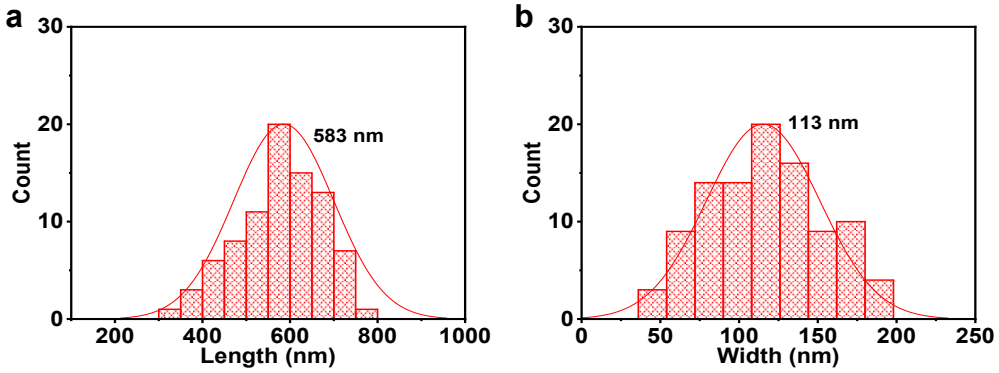

Figure S4. (a) Length and (b) width distribution of **Agg2** in MCH (c = 50 μM). The histograms were constructed from measurements of at least 100 individual assemblies.

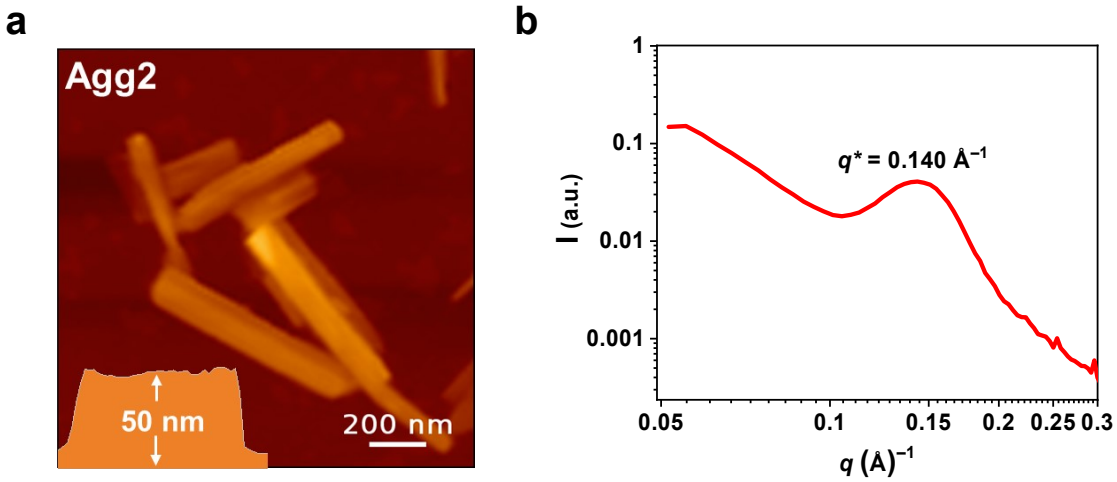

Figure S5. (a) AFM image of **Agg2** in MCH (c = 50 μM) drop-cast on a silicon wafer and (b) SAXS profile for lamellar stacking in **Agg2**.

One-dimensional SAXS profile of the **Agg2** cast film after subtraction of the blank film scattering. The lamellar correlation peak appears at $q^* \approx 0.140$ Å^{-1}, corresponding to a repeat distance of $d = 2\pi/q^* \approx 4.49$ nm. Consistently, AFM imaging reveals multilayer sheet-like assemblies with a typical deposited height of ca. 50 nm, supporting a multilayer lamellar sheet-like model for **Agg2** rather than a monolayer 2D sheet.

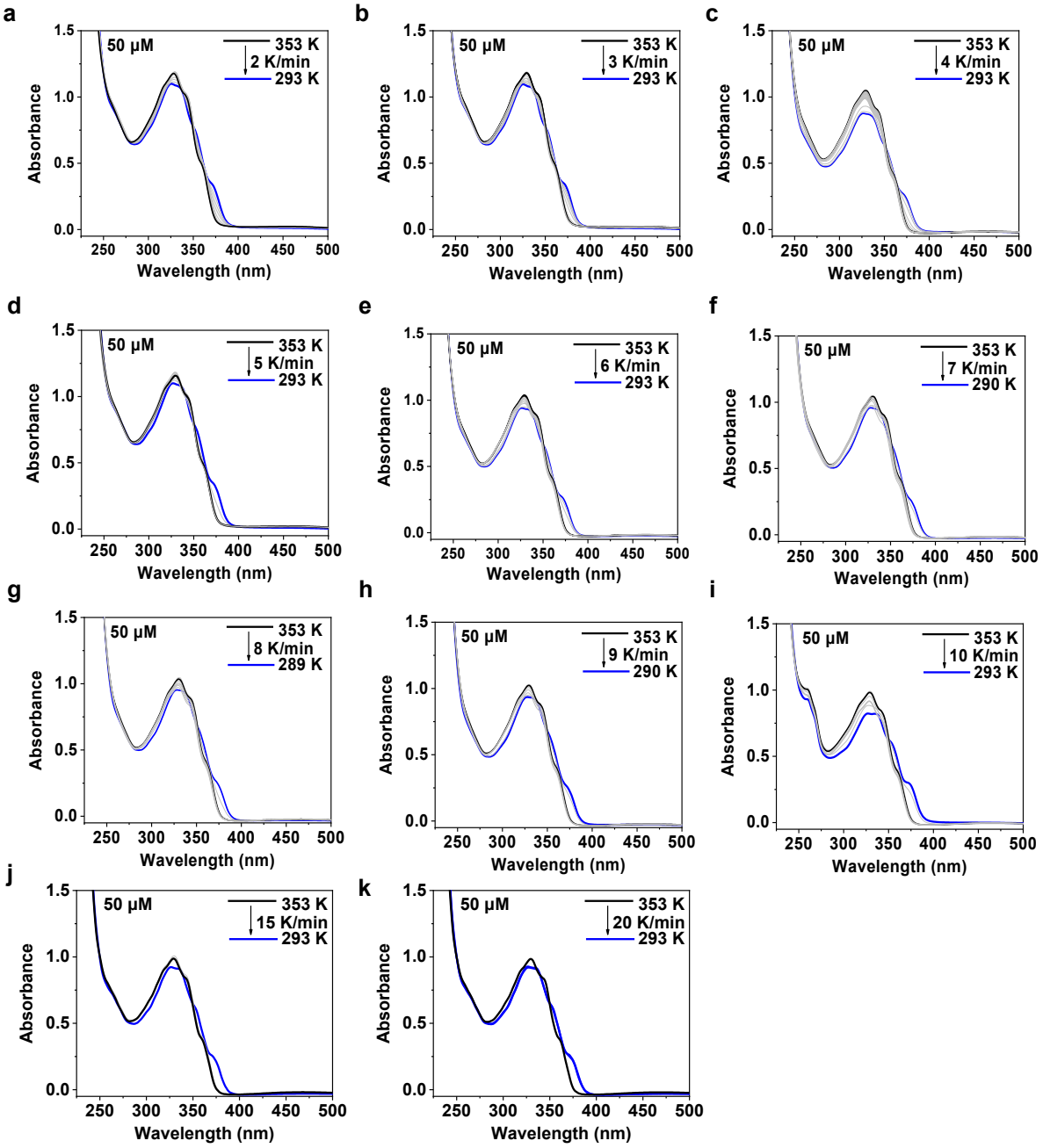

Figure S6. The VT UV–vis absorption spectra of compound **1** (c = 50 μM, MCH) at different cooling rates under no stirring: (a) 2 K/min, (b) 3 K/min, (c) 4 K/min, (d) 5 K/min, (e) 6 K/min, (f) 7 K/min, (g) 8 K/min, (h) 9 K/min, (i) 10 K/min, (j) 15 K/min, and (k) 20 K/min.

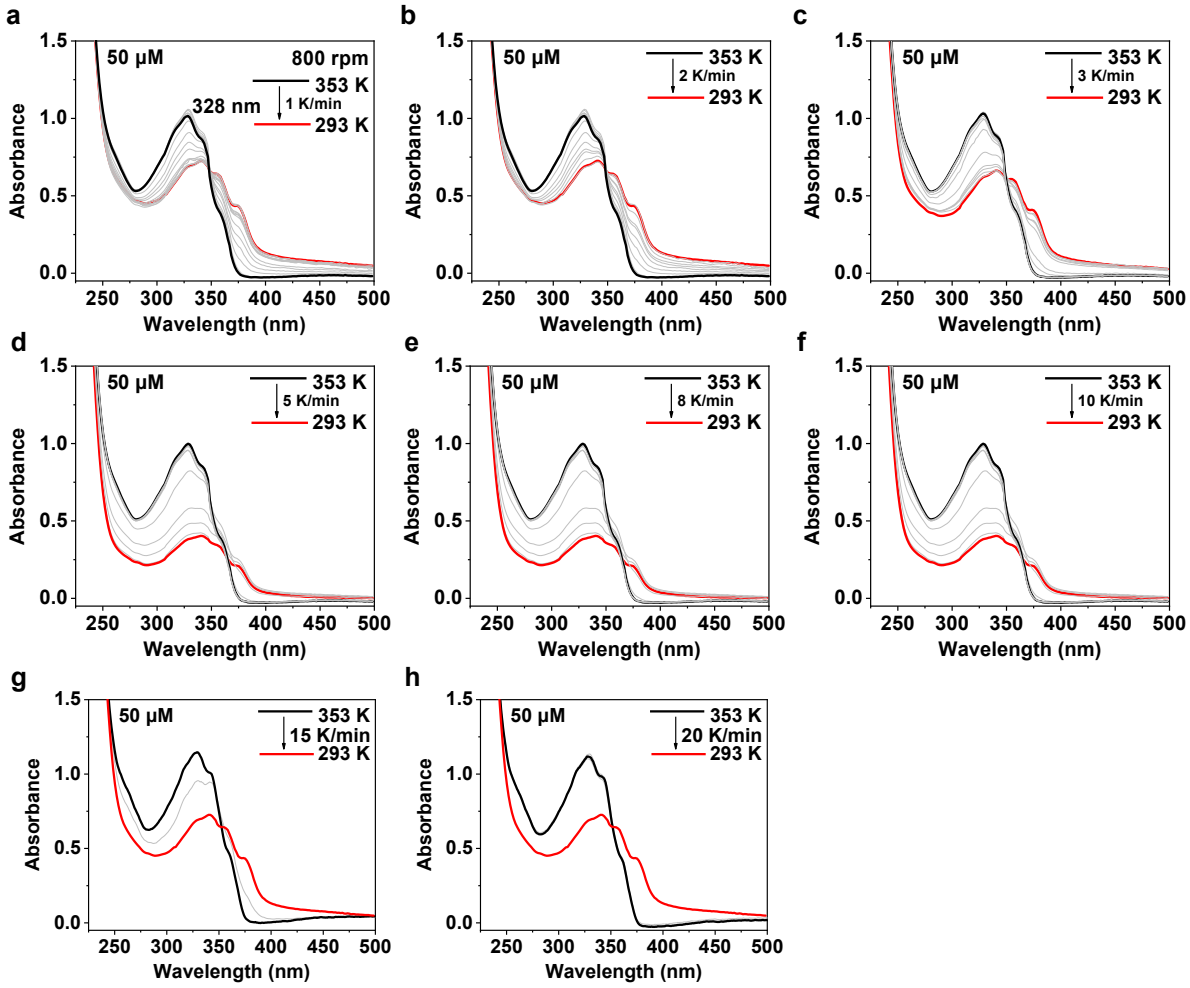

Figure S7. The VT UV–vis absorption spectra of compound **1** (c = 50 μM, MCH) at different cooling rates under stirring (800 rpm): (a) 1 K/min, (b) 2 K/min, (c) 3 K/min, (d) 5 K/min, (e) 8 K/min, (f) 10 K/min, (g) 15 K/min, and (h) 20 K/min.

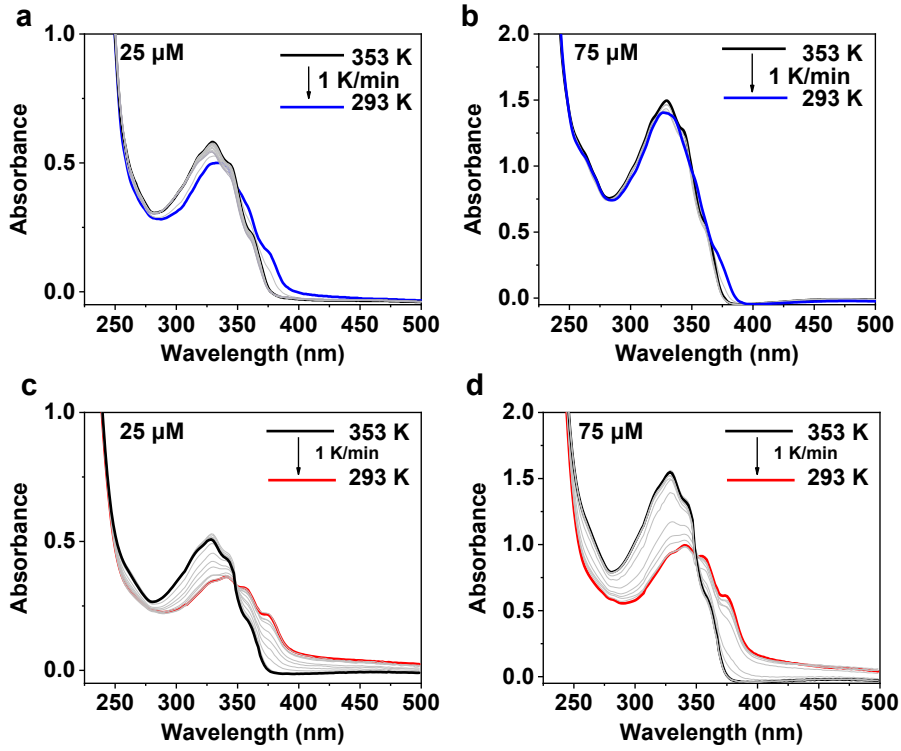

Figure S8. VT UV–vis absorption spectra of compound **1** in MCH at different concentrations during cooling from 353 to 293 K at 1 K/min: (a) 25 μM and (b) 75 μM under quiescent conditions; (c) 25 μM and (d) 75 μM under continuous stirring at 800 rpm.

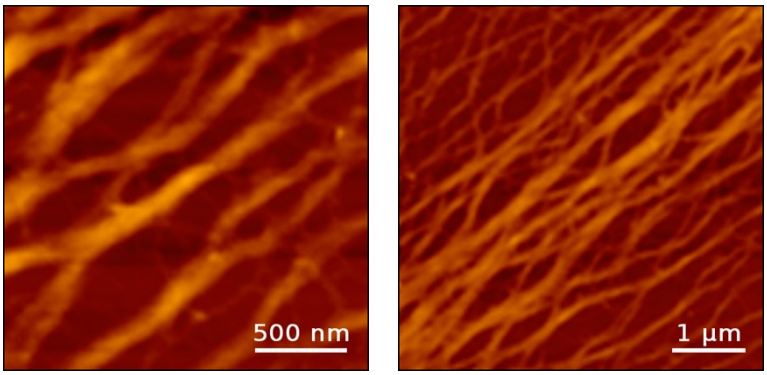

Figure S9. AFM images of **Agg1** prepared in MCH (c = 50 μM) by quiescent cooling from 353 to 293 K at 20 K/min and drop-cast onto a silicon wafer.

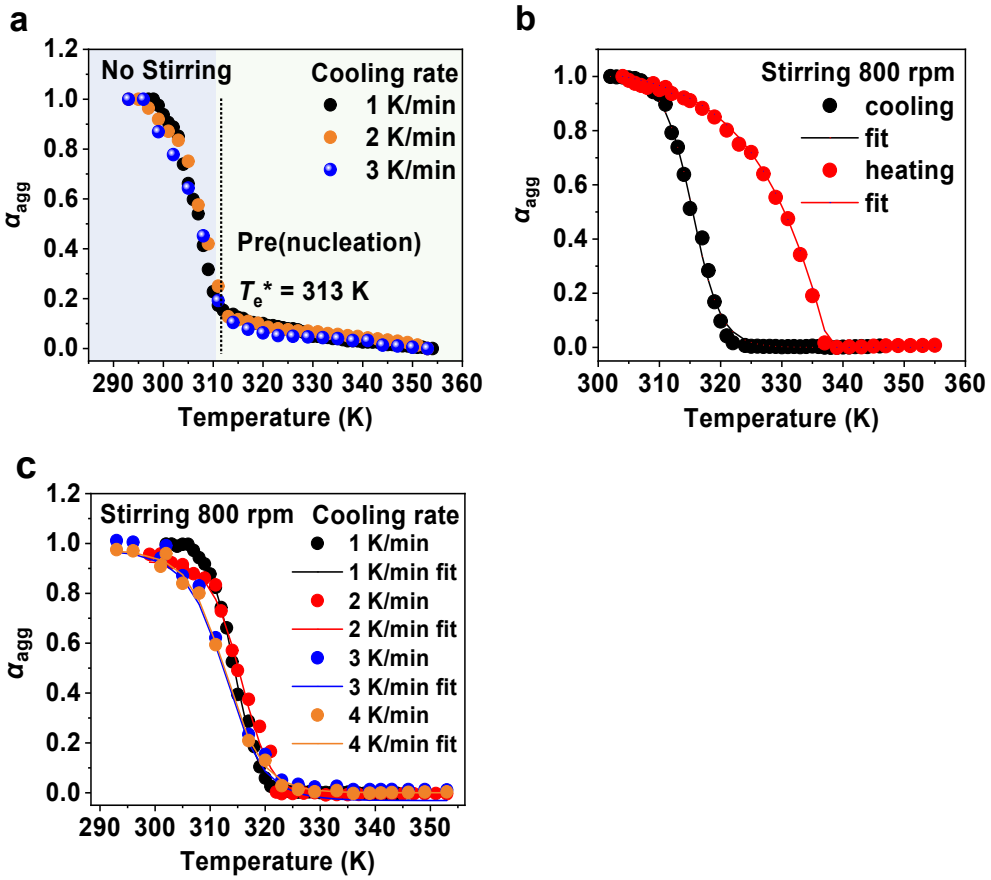

Figure S10. Temperature-dependent a_{agg} traces monitored at λ = 328 nm: (a) quiescent cooling from 353 to 293 K, derived from the VT UV–vis spectra in Fig. S6; (b) cooling (black) and heating (red) under stirring at 800 rpm; and (c) cooling under stirring at 800 rpm, derived from the VT UV–vis spectra in Fig. S7.

Table S1 Thermodynamic parameters obtained by fitting the curves in Fig. S10c with the nucleation-elongation model of compound **1**

Cooling rate K min^{-1}	Concentration μM	ΔH kJ mol^{-1}	ΔS kJ mol^{-1} K^{-1}	T_e K	ΔG_{298} kJ mol^{-1}	K_{nucl}	K_{el}	σ
1	50 μM	-340.9	-1	315.0	-42.9	1.6E-07	33866482.4	0.48
2	50 μM	-328.2	-0.961	314.2	-41.5	19167916.2	19168651.2	0.99
3	50 μM	-208.3	-0.584	312.5	-34.2	361337.6	1011879.7	0.35
4	50 μM	-233.1	-0.665	311.9	-34.9	732571.5	1332381.6	0.54

The rate dependence of the fitted parameters likely reflects non-equilibrium effects during finite-rate cooling. Faster cooling increases kinetic lag, delaying assembly growth relative to the temperature change and altering the shape of the α_{agg}–T trace. Because ΔH, ΔS and σ are strongly coupled in the fitting procedure, small changes in the trace shape can redistribute among these parameters.

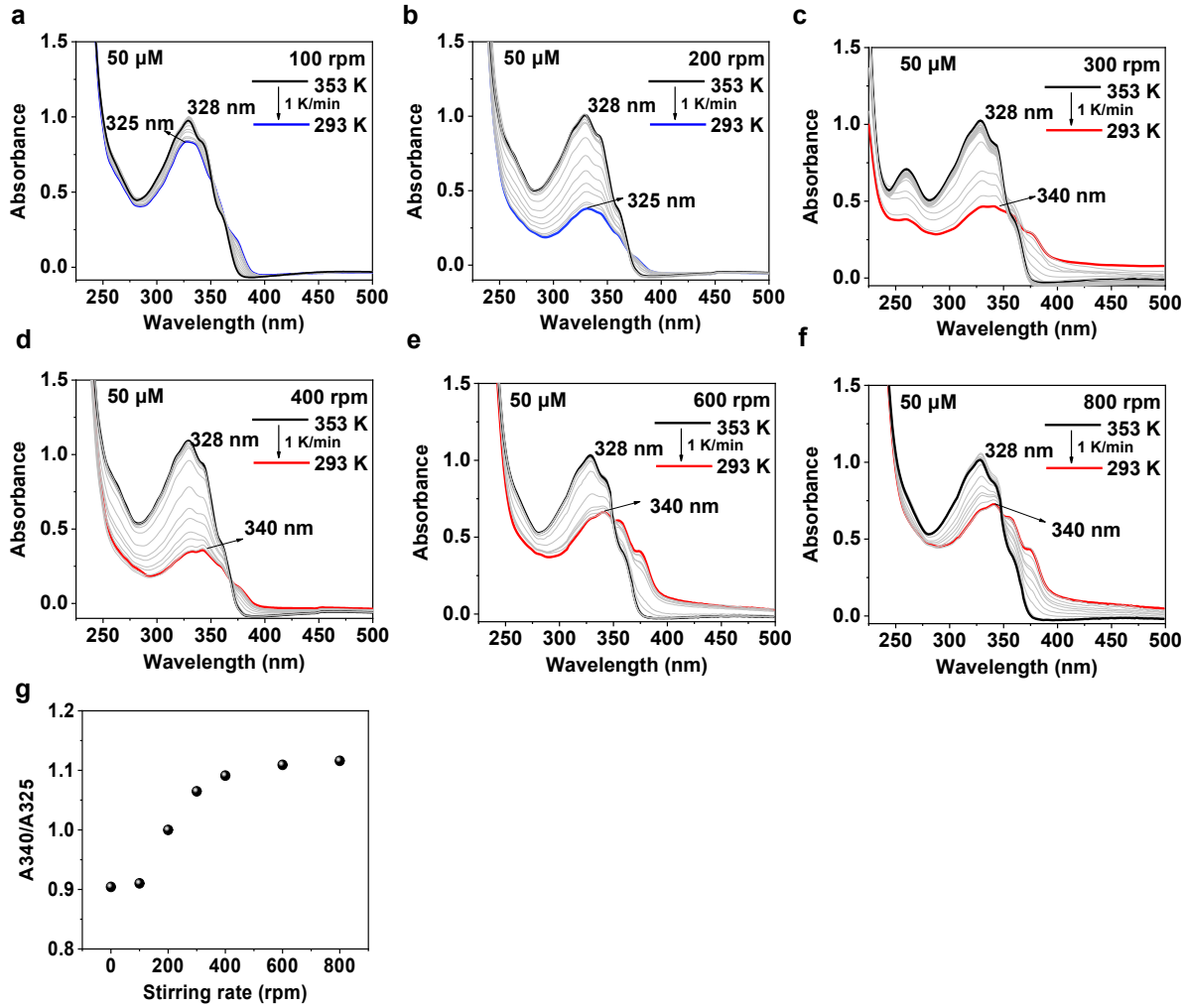

Figure S11. The VT UV–vis absorption spectra of compound **1** (c = 50 μM, MCH) with a cooling rate of 1 K/min from 353 K to 293 K under different stirring rates: (a) 100 rpm, (b) 200 rpm, (c) 300 rpm, (d) 400 rpm, (e) 600 rpm, and (f) 800 rpm. (g) UV–vis analysis of the stirring-speed-dependent transition. The absorbance ratio A340/A325 was calculated from the terminal UV–vis spectra obtained at different stirring rates. The ratio serves as a spectral indicator of **Agg2** character rather than an absolute **Agg1**/**Agg2** population fraction. The intermediate value at 200 rpm supports its assignment as a mixed transitional regime.

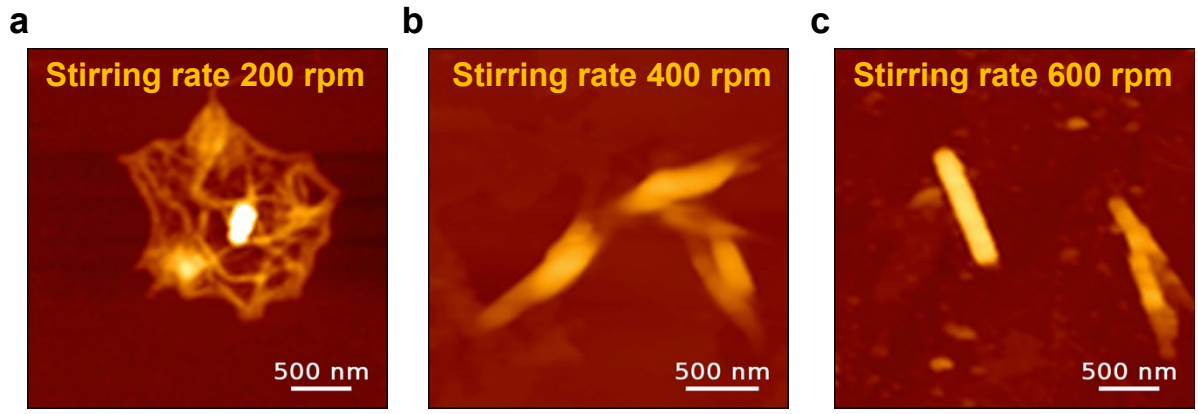

Figure S12. AFM images of samples obtained under continuous stirring at (a) 200 rpm, (b) 400 rpm, and (c) 600 rpm during cooling in MCH (c = 50 μM, 353→293 K, 1 K/min) drop-cast on a silicon wafer. The sample obtained at 200 rpm shows mixed fibrous and sheet-like morphologies, whereas the samples obtained at 400 and 600 rpm are dominated by sheet-like assemblies.

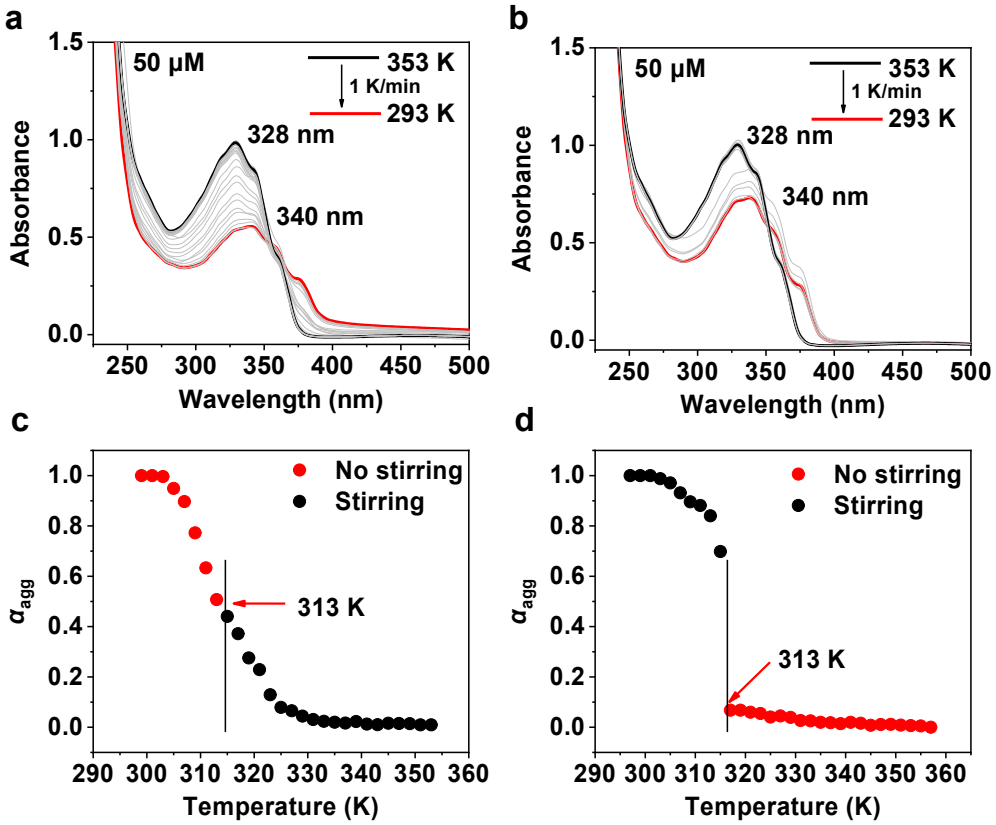

Figure S13. VT UV–vis absorption spectra of compound **1** (c = 50 μM in MCH) recorded upon cooling from 353 K to 293 K at 1 K/min under different stirring windows (800 rpm): (a) stirring applied during 353–313 K, (b) stirring applied during 313–293 K. Temperature-dependent changes in the α_{agg} monitored at 328 nm for the corresponding experiments: (c) stirring applied during 353–313 K and (d) stirring applied during 313–293 K.

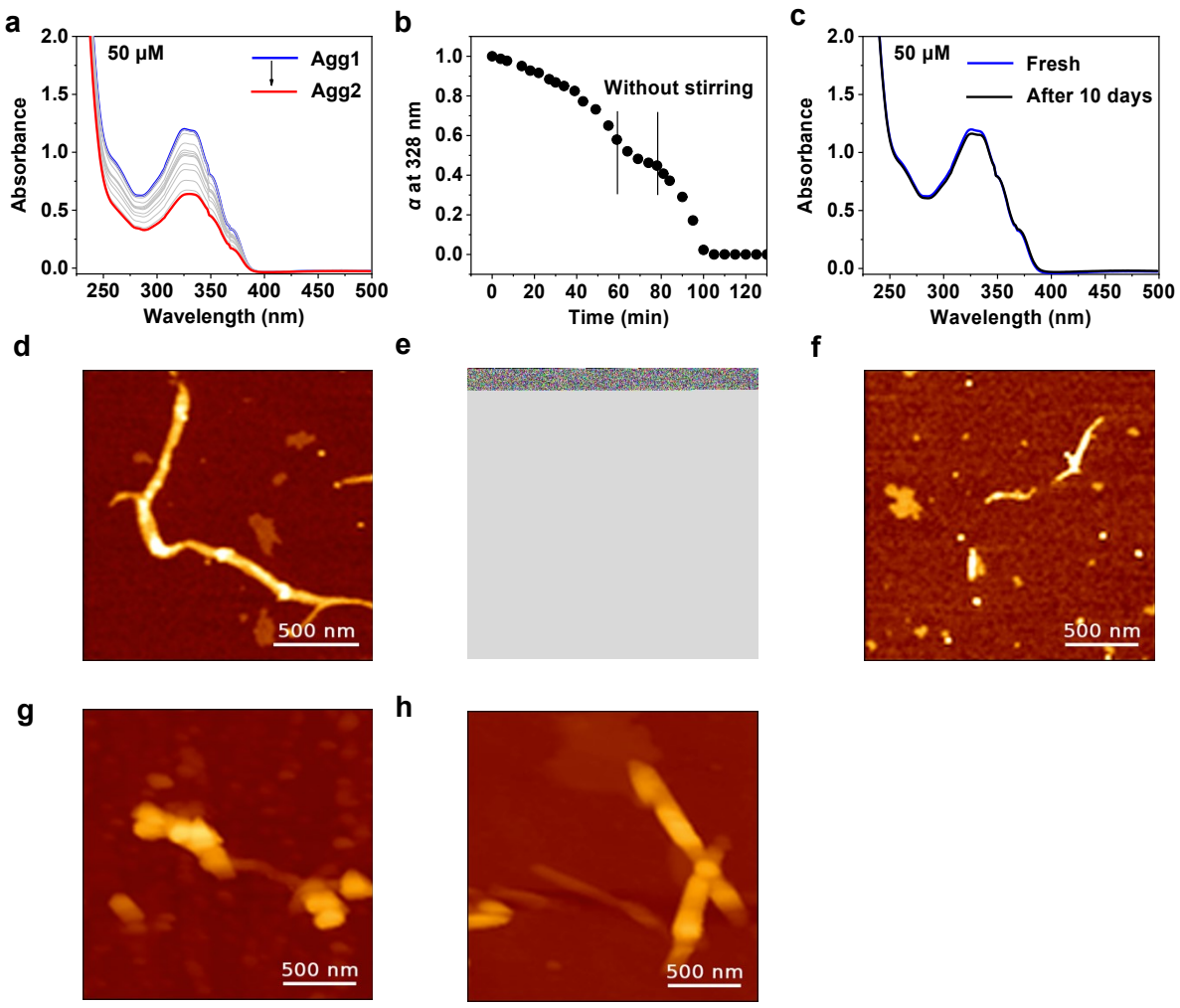

Figure S14. (a) Time-dependent UV–vis absorption spectra recorded during the **Agg1**-to-**Agg2** transformation at 298 K under stirring. Stirring was temporarily stopped between 60 and 80 min and then resumed. (b) Time evolution of the absorbance at 328 nm for the same experiment. The spectral evolution slowed during the no-stirring interval and increased again after stirring was resumed. (c) UV–vis absorption spectra of freshly prepared **Agg1** and of **Agg1** after standing for 10 days at 298 K and 50 μM without stirring. (d) AFM image of **Agg1** after standing without stirring in MCH (c = 50 μM) at 298 K for 1 day. The sample was drop-cast onto a silicon wafer before imaging. (e–h) Representative AFM images collected during the **Agg1**-to-**Agg2** conversion in MCH (c = 50 μM) at 298 K: (e) 0 min, initial nanofibers **Agg1**; (f) 30 min, disrupted nanofibers structures; (g) 60 min, particle-like or irregular species; and (h) 90 min, sheet-like assemblies. Samples were drop-cast onto silicon wafers before imaging.

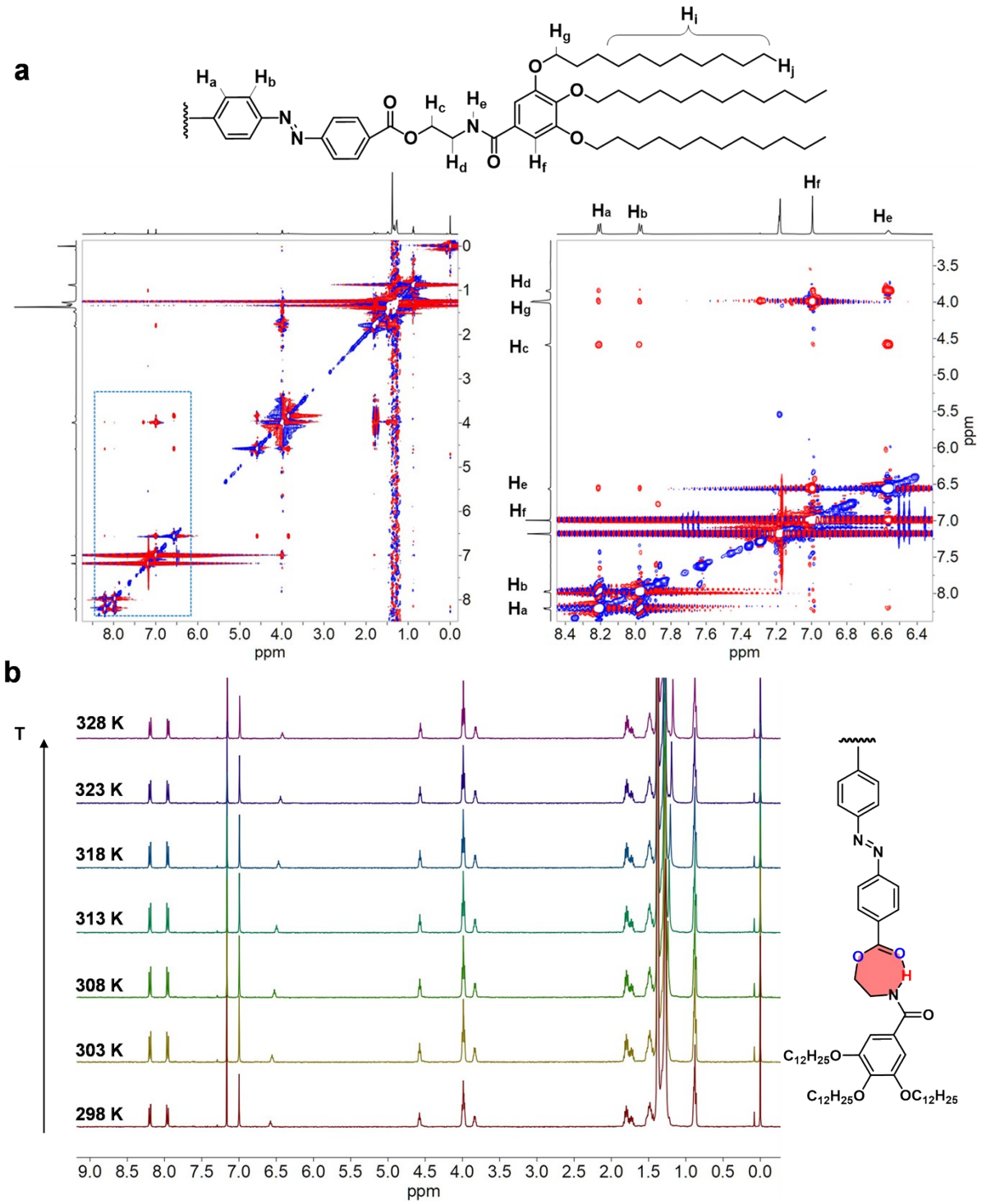

Figure S15. (a) Full (left) and expanded (right) 2D ROESY NMR spectra of **1** (600 MHz, 298 K, c = 1 mM), showing magnified views of the regions marked by blue squares. (b) VT ^{1}H NMR spectra of **1** (400 MHz, c = 1 mM) in $CDCl_3$/cyclohexane-d_{12} (v/v = 30/70). The samples were prepared by dissolving the solid compound in $CDCl_3$, followed by rapid addition of cyclohexane-d_{12}.

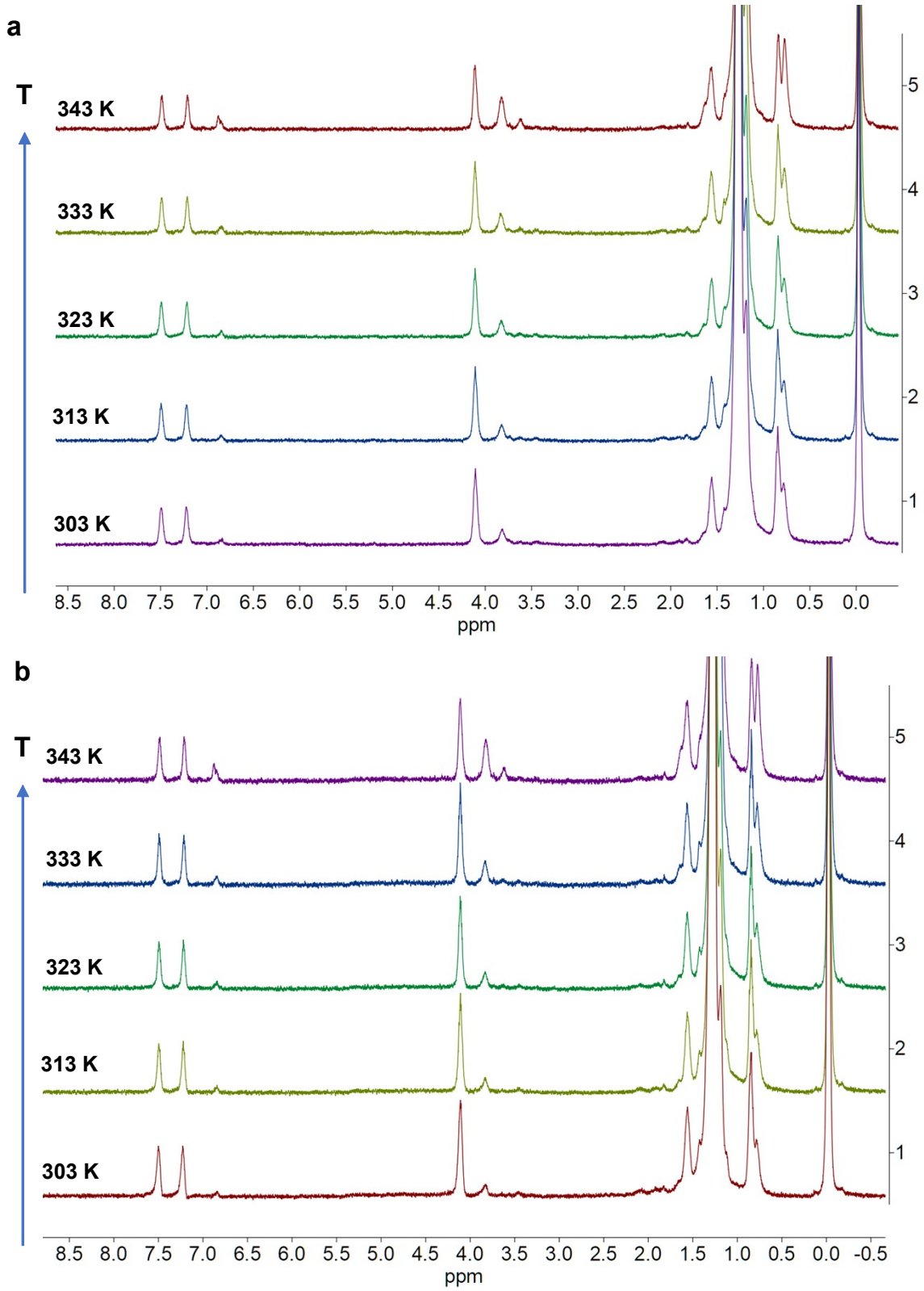

Figure S16. (a) **Agg1** and (b) **Agg2** VT ^{1}H NMR spectra (400 MHz, c = **1** mM) in cyclohexane-d_{12}.

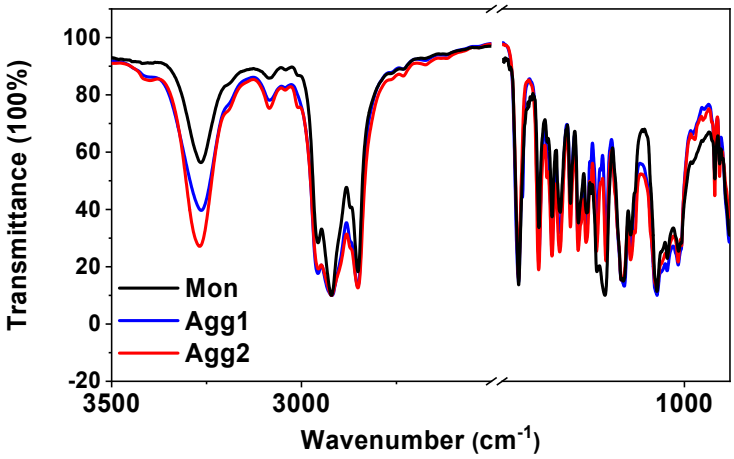

Figure S17. FT-IR spectra of the monomer, **Agg1** and **Agg2** in MCH (c = 1 mM).

FTIR spectra show only minor shifts of the amide-related bands among **Mon**, **Agg1** and **Agg2**, indicating that the overall hydrogen-bond strength does not change dramatically upon assembly. Instead, the aggregation states mainly differ in the distribution of local amide environments, as reflected by changes in band broadening. Consistently, variable-temperature ^{1}H NMR spectra exhibit only small chemical-shift changes under the NMR conditions. In contrast, 2D NMR (2D-ROESY) reveals through-space contacts consistent with possible intramolecular contacts, including amide-related interactions. Together, these data suggest possible intramolecular contacts and different local amide environments, but they do not provide a direct structural assignment of **Agg1** or **Agg2** in solution.

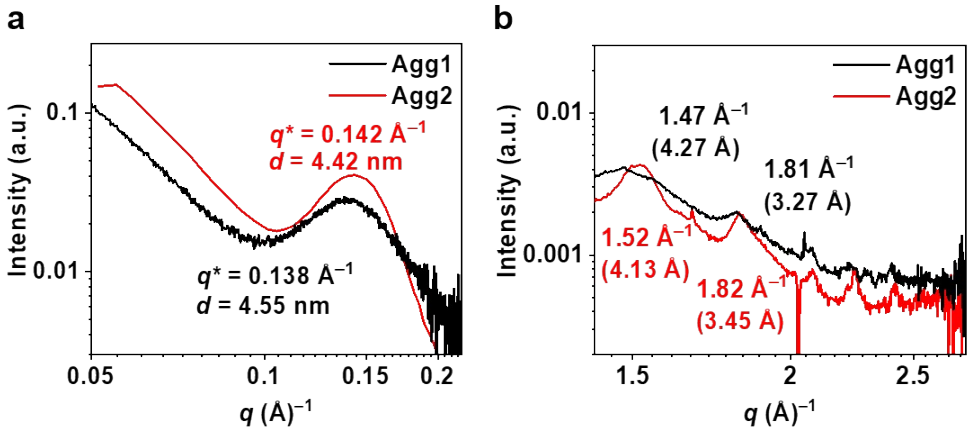

Figure S18. (a) SAXS profiles showing a principal lamellar correlation peak (q*) at 0.138 Å^{-1} for **Agg1** and 0.142 Å^{-1} for **Agg2**, corresponding to d–spacings of 4.55 and 4.42 nm, respectively. (b) WAXS profiles showing reflections at q = 1.47 and 1.52 Å^{-1}, corresponding to d–spacings of 4.27 and 4.13 Å, respectively, consistent with short–range alkyl/side–chain packing, and reflections at q = 1.81 and 1.82 Å^{-1}, corresponding to d–spacings of 3.47 and 3.45 Å, respectively, consistent with π–π stacking of the aromatic/azo units.

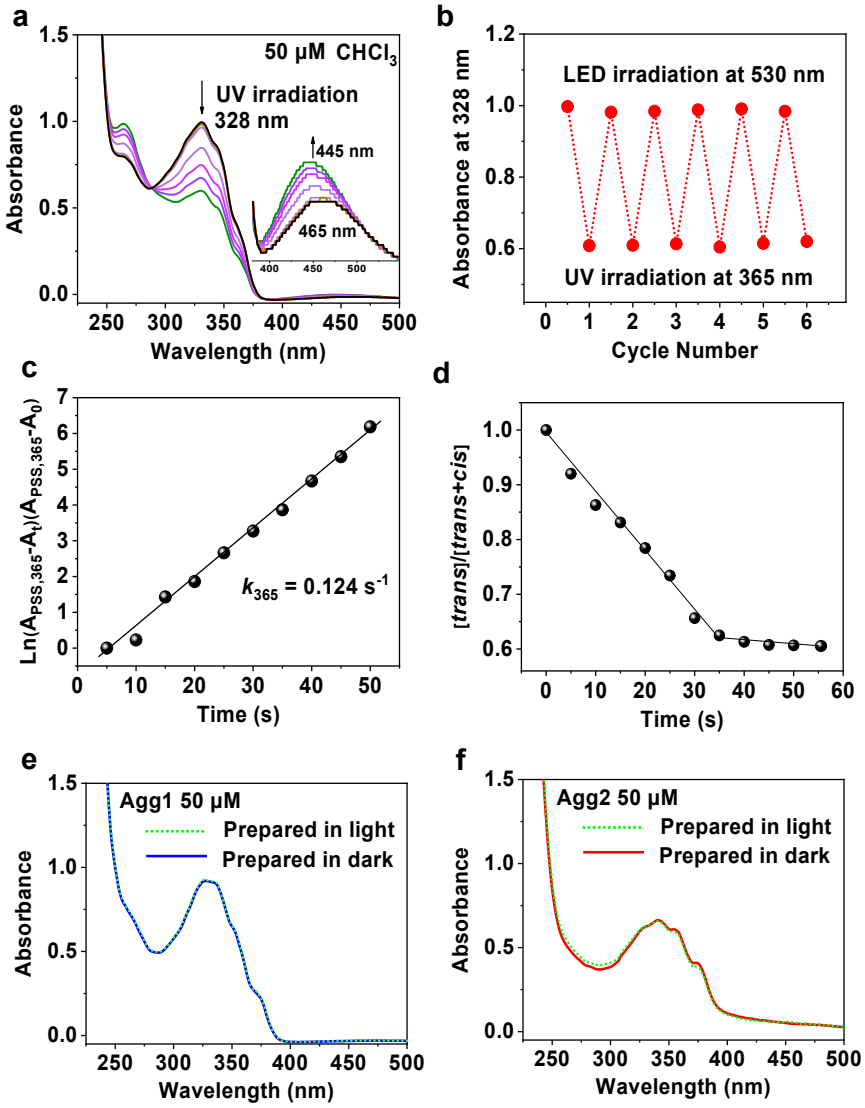

Figure S19. (a) UV–vis absorption spectra of **1** in $CHCl_3$ and the spectral evolution under 365 nm irradiation. (b) Reversible photoisomerization cycling under alternating irradiation at 365 and 530 nm (six cycles). (c) First-order kinetic fitting of the *trans*→*cis* photoisomerization under 365 nm irradiation, giving k_{365} from the slope. (d) Time-dependent change in the relative fraction of *trans*-**1** during 365 nm irradiation, estimated from the absorbance variation at 328 nm. (e, f) Light/dark control experiments for the assembly of compound **1** in MCH under quiescent and stirred cooling conditions. The quiescent samples gave **Agg1** spectra, whereas the stirred samples gave **Agg2** spectra, indicating that the **Agg1**/**Agg2** selection is not photoisomerization-driven under the present assembly conditions.

The photoisomerization of this compound was investigated in $CHCl_3$. Upon irradiation of **1** in $CHCl_3$ at 365 nm for 1 min, the band at 328 nm decreased and the spectrum reached a photostationary state (PSS_{365}), consistent with the formation of a *trans*/*cis* mixture. Alternating irradiation at 365 and 530 nm over six cycles produced reversible spectral changes without obvious fatigue, indicating good photoswitching reversibility under these conditions. Analysis of the time-dependent absorbance trace at 328 nm gave an apparent *trans*→*cis* photoisomerization rate constant of $k_{365} = 0.124\ s^{-1}$, and the composition at PSS_{365} was estimated to be *trans*/*cis* = 56/44. Since *cis*-**1** could not be obtained in sufficiently high purity under these conditions, the self-assembly studies discussed focus on *trans*-**1**.

4. Collection of Spectra

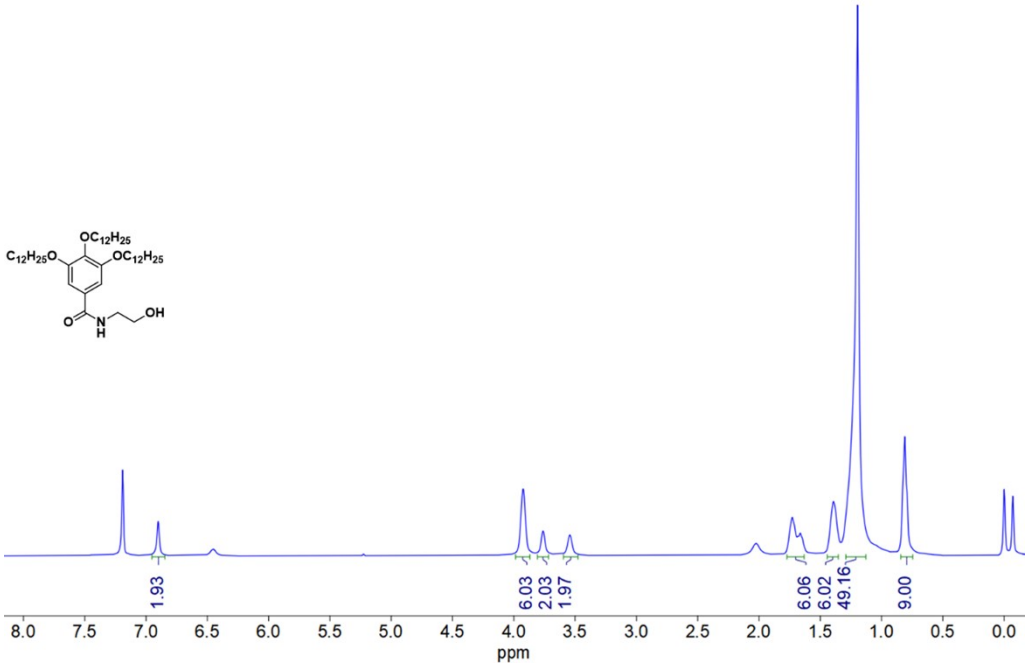

Figure S20. ^{1}H NMR spectrum of compound **Z-2** (400 MHz, $CDCl_3$, 298 K)

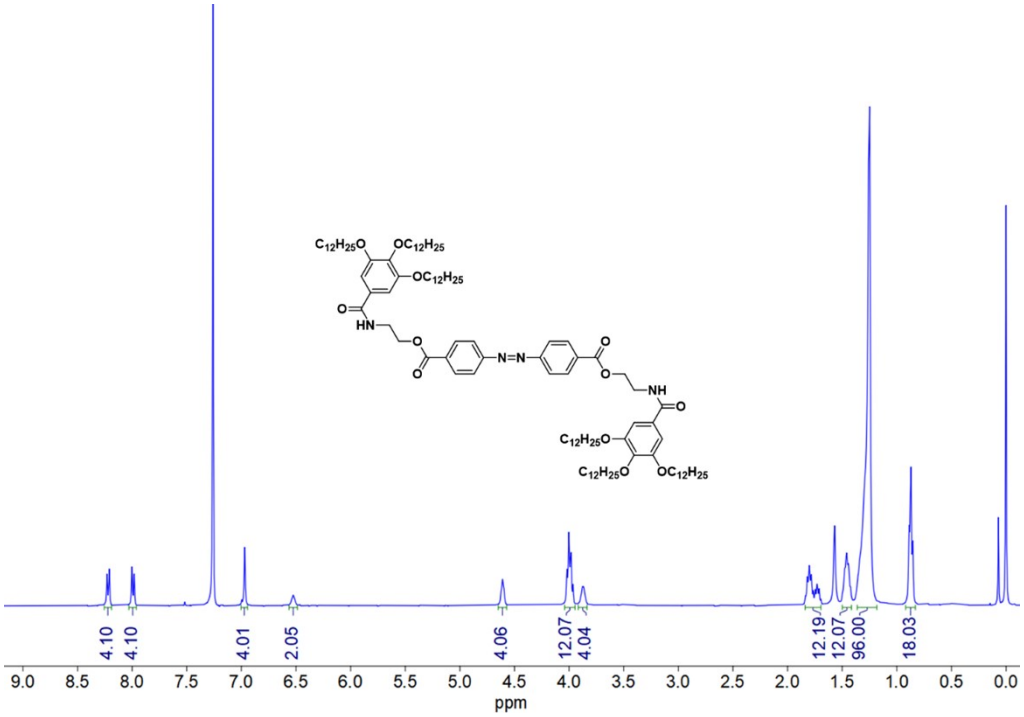

Figure S21. ^{1}H NMR spectrum of compound **1** (400 MHz, $CDCl_3$, 298 K)

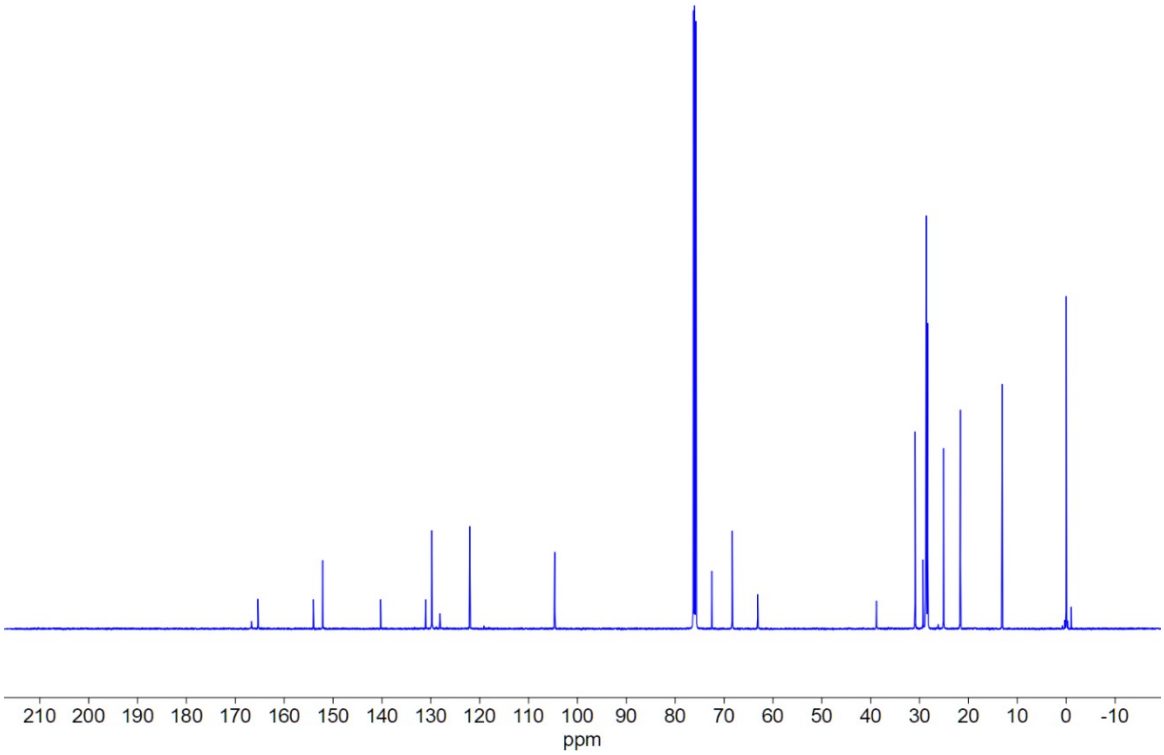

Figure S22. ^{13}C NMR spectrum of compound **1** (126 MHz, $CDCl_3$, 298 K)

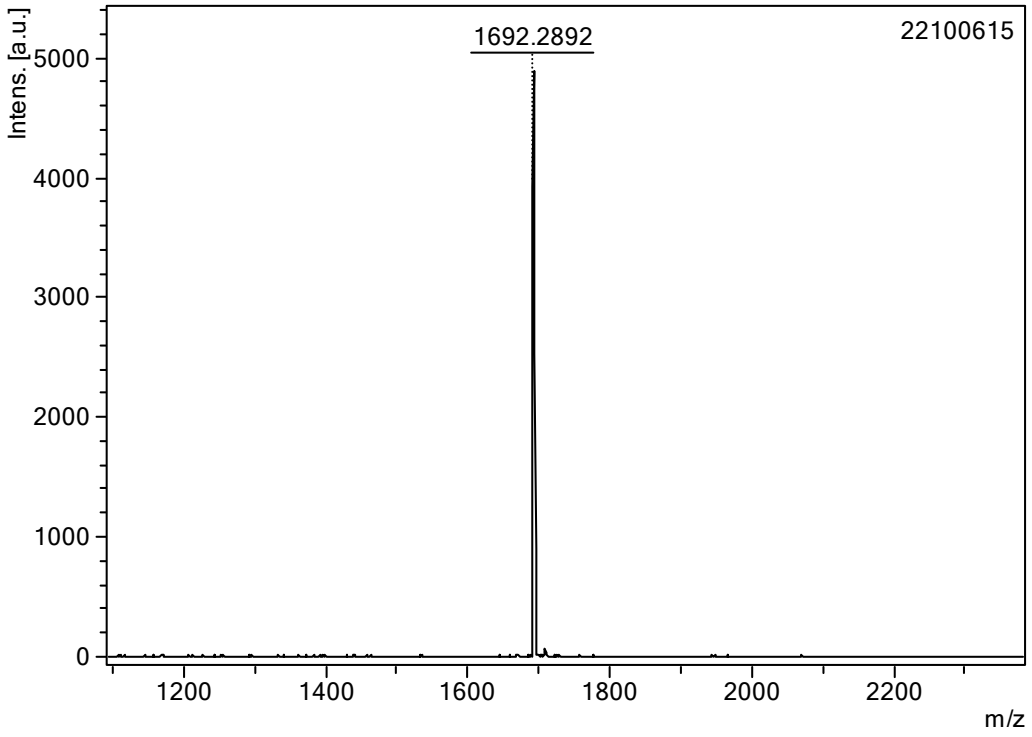

Figure S23. MS spectrum of compound **1**

5. References

[1] Y. Zhang, Y. Q. Feng, J. H. Wang, G. Han, M. Y. Li, Y. Xia, Z. D. Feng, RSC Adv. 2017, 7, 35672-35680.

[2] E. E. Greciano, B. Matarranz, L. Sánchez, Angew. Chem. Int. Ed. 2018, 57, 4697-4701.

[3] A. J. Markvoort, H. M. ten Eikelder, P. A. Hilbers, T. F. de Greef, E. W. Meijer, Nat. Commun. 2011, 2, 509.

[4] H. M. ten Eikelder, A. J. Markvoort, T. F. de Greef, P. A. Hilbers, J. Phys. Chem. B 2012, 116, 5291-5301.

[5] X. Q. Xue, J. Zhu, Z. B. Zhang, N. C. Zhou, X. L. Zhu, React. Funct. Polym. 2010, 70, 456-462.

[6] W. Lu, Y. Y. Feng, C. Cao, M. Li, E. Z. Liu, S. P. Li, C. Q. Qin, W. P. Hu, W. Feng, J. Mater. Chem. A 2015, 3, 11787-11795.